Polymer Chemistry

Degradable Sugar-based Magnetic Hybrid Nanoparticles for Recovery of Crude Oil from Aqueous Environments

Journal:	*Polymer Chemistry*
Manuscript ID	PY-ART-01-2020-000029.R1
Article Type:	Paper
Date Submitted by the Author:	11-Feb-2020
Complete List of Authors:	Dong, Mei; Texas A&M University, Chemistry Song, Yue; Texas A&M University, Chemistry Wang, Hai; Texas A&M University, Chemistry Su, Lu; Texas A&M University, Chemistry Shen, Yidan; Texas A&M University, Chemistry Tran, David; Texas A&M University, Chemistry Letteri, Rachel; Texas A&M University, Flores, Jeniree; Texas A&M University, Chemistry Lin, Yen-Nan; Texas A&M University, Chemistry Li, Jialuo; Texas A&M University, Chemistry Wooley, Karen; Texas A&M University, Chemistry

ARTICLE

Degradable Sugar-based Magnetic Hybrid Nanoparticles for Recovery of Crude Oil from Aqueous Environments

Received 00th January 20xx,
Accepted 00th January 20xx

DOI: 10.1039/x0xx00000x

Mei Dong,[a] Yue Song,[a] Hai Wang,[a] Lu Su,[a] Yidan Shen,[b] David K. Tran,[a] Rachel A. Letteri,[a] Jeniree A. Flores,[a] Yen-Nan Lin,[a,d] Jialuo Li,[a] and Karen L. Wooley*[,a,b,c]

In this work, we designed and fabricated a nanoscopic sugar-based magnetic hybrid material that is capable of tackling environmental pollution posed by marine oil spills, while minimizing potential secondary problems that may occur from microplastic contamination. These readily-defined magnetic nanocomposites were constructed through co-assembly of magnetic iron oxide nanoparticles (MIONs) and a degradable amphiphilic polymer, poly(ethylene glycol)-*b*-dopamine-functionalized poly(ethyl propargyl glucose carbonate)-*b*-poly(ethyl glucose carbonate), PEG-*b*-PGC[(EPC-MPA)-*co*-(EPC-DOPA)]-*b*-PGC(EC), driven by supramolecular co-assembly in water with enhanced interactions provided *via* complexation between dopamine and MIONs. The composite nanoscopic assemblies possessed a *pseudo*-micellar structure, with MIONs trapped within the polymer framework. The triblock terpolymer was synthesized by sequential ring-opening polymerizations (ROPs) of two glucose-derived carbonate monomers, initiated by a PEG macroinitiator. Dopamine anchoring groups were subsequently installed by first introducing carboxylic acid groups using a thiol-yne click reaction, followed by amidation with dopamine. The resulting amphiphilic triblock terpolymers and MIONs were co-assembled to afford hybrid nanocomposites using solvent exchange processes from organic solvent to water. In combination with hydrophobic interactions, the linkage between dopamine and iron oxide stabilized the overall nanoscopic structure to allow for the establishment of a uniform globular morphology, whereas attempts at co-assembly with the triblock terpolymer precursor, lacking dopamine side chains, failed to afford well-defined nanostructures. The magnetic hybrid nanoparticles demonstrated high oil sorption capacities, *ca.* 8 times their initial dry weight, attributed, in part, to large surface areas leading to effective contact between the nanomaterials and hydrocarbon pollutants. Moreover, the naturally-derived polymer framework undergoes hydrolytic degradation to break down into byproducts that include glucose, ethanol and dopamine if not recovered after deployment, alleviating concerns of potential microplastic generation and persistence.

Introduction

Oil spills endanger marine and human life, threaten drinking water and natural resources, damage parts of the food chain, and pose serious hazards to the aquatic environment, public health, and global economy.[1-3] Several methods (*e.g.* physical, mechanical, chemical and biological, *etc.*) are available to contain oil spills in addition to natural processes, such as evaporation, oxidation, and biodegradation.[4, 5] Common physical methods for oil spill clean-up include pressure washing, raking and bulldozing, which are time-consuming and require extensive equipment and personnel resources. Mechanical containment methods, such as booms and skimmers, are used at an earlier stage to block the spread of oil, limit its area, and remove it from the water.[4] Chemical and biological treatment of oil, such as dispersing agents and gelling agents, can be used followed by, or even in place of, mechanical methods, especially in areas where untreated oil may reach shorelines and in sensitive habitats where clean-up processes become difficult and environmentally damaging.[6, 7] Among these methods and techniques, synthetic sorbents and dispersing agents are more attractive and commonly used to remove final traces of oil or to remove oil in areas where mechanical containment and clean-up are difficult.[8, 9]

With the growing awareness of the persistence of plastics in the environment, including microplastics, there has been a rising concern about the materials used in the commercially-available sorbents and dispersing agents on the market.[10-13] Synthetic polymer-based sorbents or dispersants have been reported to generate micro- and nano-plastics in aquatic environments.[14-16] Transfer of these persistent micro- and nano-plastics across the food chain can cause serious and far-reaching threat to the global health of wildlife and human populations.[13, 14, 17] Moreover, agents that are deployed are often not recovered, which may not only contribute to the contamination but also represent a wasteful approach to material resources, as occurs for a traditional linear, take-make-dispose economy.[18] One of the key strategies to solve these problems is the development of materials that can undergo passive degradation if discarded and active recycling or upcycling processes if recovered. By such processes, it is possible to evolve towards a

[a] *Department of Chemistry, Texas A&M University, College Station, Texas 77843, United States*
[b] *Department of Materials Science & Engineering, Texas A&M University, College Station, Texas 77843, United States*
[c] *Department of Chemical Engineering, Texas A&M University, College Station, Texas 77842, United States*
[d] *College of Medicine, Texas A&M University, Bryan, Texas 77807, United States.*
† Electronic Supplementary Information (ESI) available: Synthetic procedures, experimental details, plots, tables, spectra, supplementary figures, and video clips. See DOI: 10.1039/x0xx00000x

more sustainable circular economic system, in which plastics can be make-use-reuse with reduction of waste.[19-21]

In addition to long-term environmental problems, previous synthetic polymeric sorbents present several challenges that include difficulty in retrieval from water, proper storage after use, and thorough cleaning for reuse, even though they demonstrate outstanding performance in pollutant absorption.[22-25] To address these limitations, magnetic actuation has been introduced to facilitate the collection of deployed conventional oil sorbents.[26-30] For instance, Gui and co-workers reported the fabrication of magnetic carbon nanotube sponges that have porous structures consisting of interconnected carbon nanotubes with Fe encapsulation.[28] Pan and co-workers designed a series of ultralow-density Fe_2O_3/C, Co/C, and Ni/C magnetic poly(acrylic acid) (PAA)-grafted polyurethane foams modified by reaction with methyltrichlorosilane for oil-water separation.[31]

Dispersed, discrete nanoparticles are expected to exhibit optimal small molecule uptake performance because they have high surface areas for contact, while maintaining adequate core volume for packaging of hydrophobic hydrocarbon components of crude oil or other pollutants. It is a common observation that oil, when spilled on water, tends to spread on the water surface in the form of a thin continuous layer of less than 5 µm thickness within a short time.[32, 33] Therefore, a large surface area-to-volume ratio is likely to be beneficial to increase the efficiency and lower the amount of absorbent required, which may also reduce the energy and economic costs.[34-36] Moreover, the existence of submarine seepage during offshore drilling operations can cause long-term damage to the environment.[37] Amphiphilic dispersant-based materials have potential to recover both surface and sub-surface oil populations.[38, 39] Assimilating all of these factors, a degradable magnetically-active dispersant-based material is considered to be highly desirable for the design of oil recovery materials, which may have limited adverse environmental impact, themselves, while also contributing to a plastic circular economy.

Previously, well-defined magnetic shell cross-linked knedel-like nanoparticles (MSCKs) were constructed through the co-assembly and intramicellar cross-linking of amphiphilic block copolymers poly(acrylic acid)$_{20}$-*block*-polystyrene$_{280}$ (PAA_{20}-*b*-PS_{280}) and oleic acid-stabilized MIONs.[34] The co-assembly process provided a large number of magnetic nanoparticles incorporated non-covalently within each polymeric micelle formed by PAA_{20}-*b*-PS_{280}, which was further cross-linked to increase stability and loading capability by creating a sturdy vessel that could undergo reversible expansion and contraction. However, the polymeric scaffold in this former design was comprised of two non-degradable components, PAA and PS, which have been widely used in cosmetics, personal care, and plastics industries for years and present an emerging threat in marine and aquatic ecosystems as microplastics.[40] To tackle these environmental concerns, our group has developed glucose-derived polycarbonates containing labile carbonate linkages to construct functional materials that are able to degrade into natural products, including glucose, carbon dioxide, and ethanol.[41-43] In this current

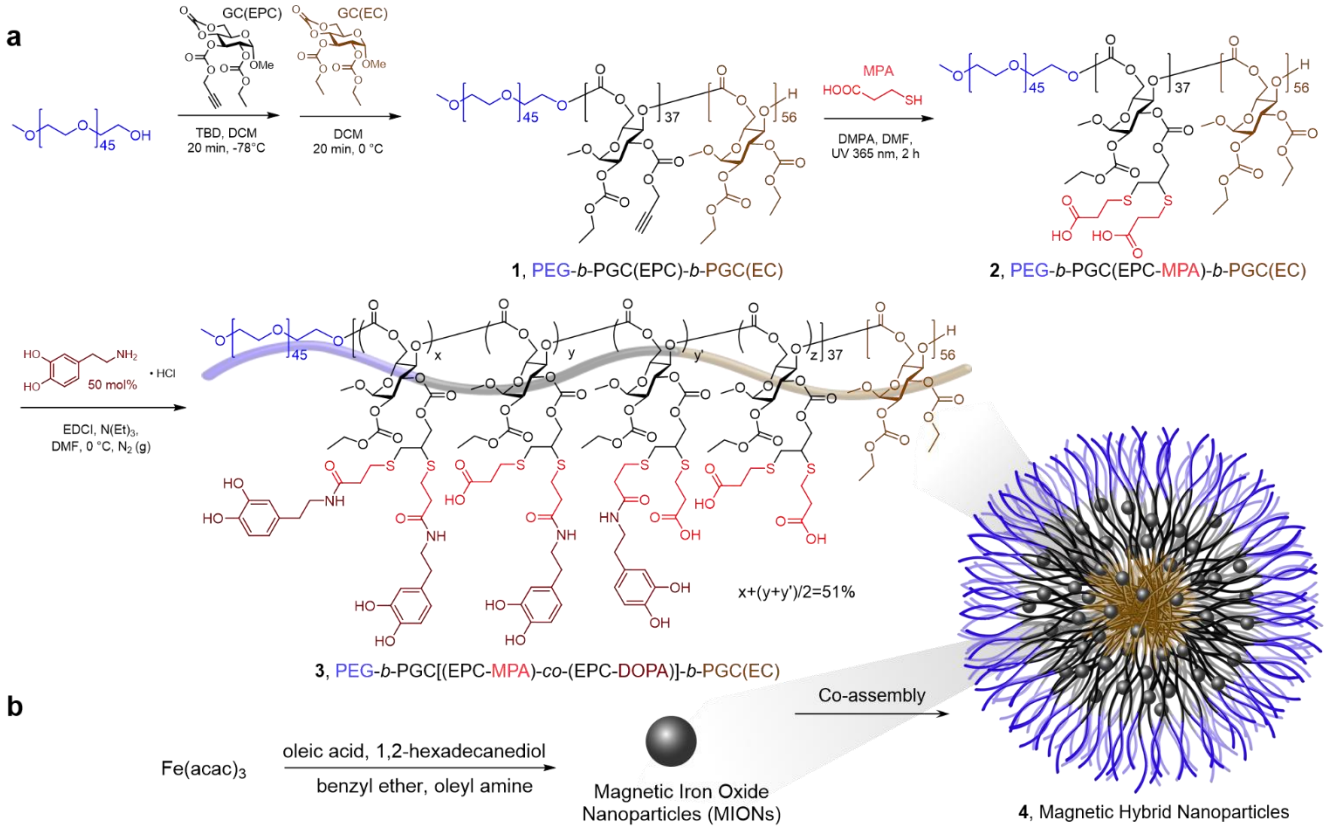

Scheme 1 (a) Synthesis of polymer **1**, PEG-*b*-PGC(EPC)-*b*-PGC(EC) by sequential ROPs of glucose carbonate monomers from a PEG macroinitiator, followed by post-polymerization modification *via* thiol-yne reaction with 3-mercaptopropionic acid (MPA) to prepare polymer **2**, PEG-*b*-PGC(EPC-MPA)-*b*-PGC(EC), and functionalization of polymer **2** with dopamine hydrochloride to afford polymer **3**, PEG-*b*-PGC[(EPC-MPA)-*co*-(EPC-DOPA)]-*b*-PGC(EC). (b) Synthesis of magnetic iron oxide nanoparticles (MIONs), and co-assembly of **3** and MIONs to afford magnetic hybrid nanoparticles **4**.

work, we have taken advantage of several interesting recent developments toward chemistries[44-46] that allow for the preparation of degradable polycarbonates containing diverse functional groups and derived from natural products,[47-56] to design a sustainable polycarbonate system that incorporates glucose, ethanol and dopamine as natural building blocks to assemble hybrid inorganic-organic nanoparticles that achieve effective oil uptake performance due to steric bulk and hydrophobicity, with magnetic recovery, and hydrolytic degradability.

Results and discussion

Design of the sugar-based magnetic hybrid nanoparticles

The magnetic nanocomposites were constructed by an overall three step sequence that involved independent preparation of amphiphilic triblock terpolymers, poly(ethylene glycol)-*b*-dopamine-functionalized poly(ethyl propargyl glucose carbonate)-*b*-poly(ethyl glucose carbonate, PEG-*b*-PGC[(EPC-MPA)-*co*-(EPC-DOPA)]-*b*-PGC(EC), and magnetic iron oxide nanoparticles (MIONs), followed by their co-assembly, as illustrated in **Scheme 1**. Using poly(ethylene glycol) (PEG) as the hydrophilic component and macroinitiator, sequential ring-opening polymerizations (ROPs) of two glucose-derived cyclic carbonate monomers afforded amphiphilic PEG-*b*-PGC with two hydrophobic segments carrying either ethyl+propargyl or ethyl+ethyl side chain functionalities. The resulting triblock terpolymers **1**, PEG-*b*-PGC(EPC)-*b*-PGC(EC), dispersed readily in water but were unable to produce co-assembled nanostructures with MIONs. Because it was hypothesized that the chemical composition of **1** provided insufficient interactions with MIONs, dopamine moieties were introduced as high-affinity anchor groups to facilitate MION encapsulation.[57-59] Thiol-yne click chemistry[60-62] of **1** with 3-mercaptopropionic acid (MPA) yielded intermediate **2**, PEG-*b*-PGC(EPC-MPA)-*b*-PGC(EC), which was then followed by amidation with dopamine to afford PEG-*b*-PGC[(EPC-MPA)-*co*-(EPC-DOPA)]-*b*-PGC(EC), **3**. Finally, co-assembly of **3** with MIONs upon exchange from organic solvent to water resulted in formation of the magnetic nanocomposites **4**.

Thermal synthesis of MIONs

The synthesis of MIONs was carried out following a standard air-free procedure, where a high-temperature solution-phase reaction of iron(III) acetylacetonate [Fe(acac)$_3$] and 1,2-hexadecanediol was conducted in the presence of oleic acid and oleylamine as (co-)surfactants.[63, 64] The as-synthesized MIONs were characterized by transmission electron microscopy (TEM) imaging and superconducting quantum interference device (SQUID) magnetometry measurements. TEM showed nanoparticles with a

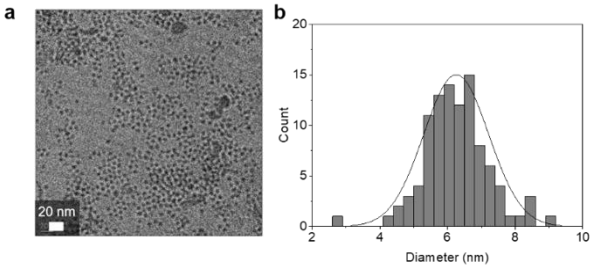

Fig. 1 (a) Transmission electron microscopy (TEM) image of MIONs. The TEM sample was drop-cast from a THF solution (*ca.* 5 mg/mL, 5 µL) with no stain; the average diameter was determined by measurement of > 100 nanoparticles. (b) Histogram of MIONs showing a D_{av} of 6 ± 1 nm.

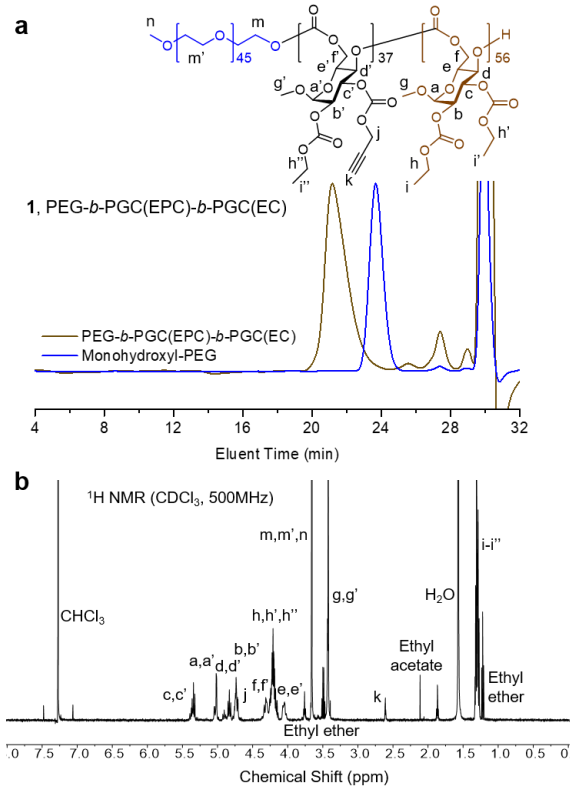

Fig. 2 (a) SEC trace (THF as eluent, 1mL/min) and (b) ^{1}H NMR (500 MHz, $CDCl_3$) spectrum of sugar-based triblock terpolymer **1** with alkyne functional groups.

number-averaged diameter (D_{av}) of 6 ± 1 nm, upon analysis of more than 100 nanoparticles (**Fig. 1**). SQUID magnetometry on MIONs indicated that the particles were in the superparamagnetic regime at room temperature, *i.e.* the particles became magnetic in the presence of an applied magnetic field, enabling magnetic separation and recycling (**Fig. S1**).

Synthesis and post-polymerization modification of functional sugar-based degradable amphiphilic block terpolymers

The functional triblock terpolymer **1** was synthesized by rapid organobase-catalyzed sequential ROPs of the glucose-based monomers GC(EPC) and GC(EC) in dichloromethane (DCM) with mPEG$_{45}$ as the hydrophilic macroinitiator and 1,5,7-triazabicyclo[4.4.0]-dec-5-ene (TBD) as the organocatalyst (**Scheme S1**). The PGC(EPC) block carried alkyne functional groups allowing for further chemical modification by click chemistry to install functionalities and afford hydrophilicity; while the PGC(EC) block was incorporated to serve as a constant hydrophobic segment. The polymerization of GC(EPC) was allowed to proceed in a -78 °C dry ice/acetone bath for 6-10 min, according to previous literature.[49] The reaction flask was then transferred to an ice water bath, the GC(EC) monomer was added, and growth of the PGC(EC) block was conducted over a period of 20 min to achieve quantitative chain extension. The reaction was quenched by adding an excess amount of acetic acid, and the polymer product was isolated by precipitation in diethyl ether three times and dried *in vacuo* to yield a white powder. Analysis of the size exclusion chromatography (SEC) trace of the resulting polymer **1** relative to that of mPEG$_{45}$ confirmed a controlled polymerization to afford a block polymer structure having an increased hydrodynamic diameter and a

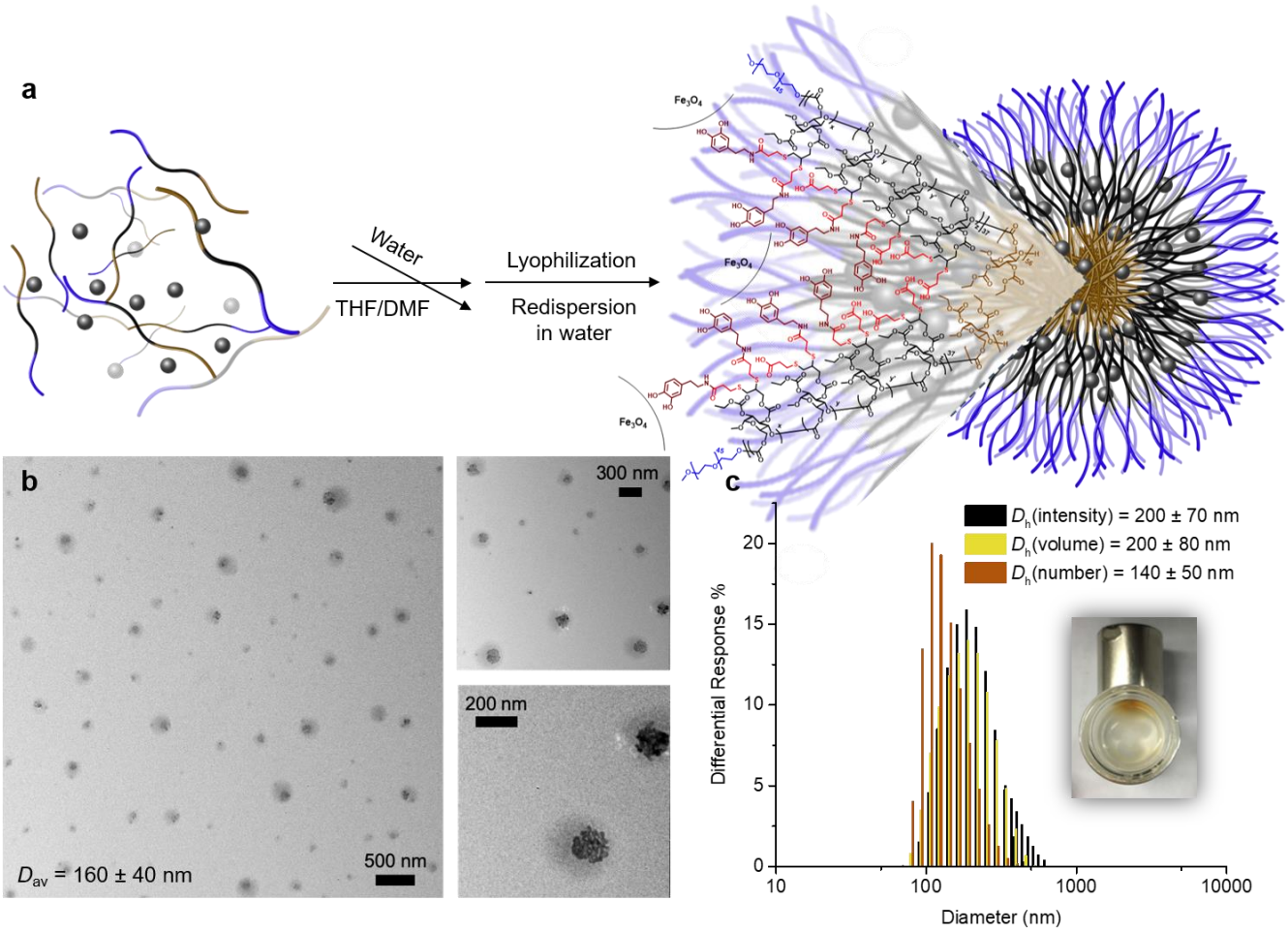

Fig. 3 (a) Schematic representation of the construction of nanocomposites **4**. (b) TEM of **4** was drop-casted from an aqueous dispersion (without stain); the scale bars in TEM images are 500, 300 and 200 nm. The average diameter was measured by counting > 50 particles. (c) Intensity-, volume-, and number-average DLS histograms of **4** dispersed in aqueous solution (*ca.* 1 mg/mL), and the inset photo shows the top view of nanocomposites **4** collected on a vial wall by application of an external magnet.

monomodal molar mass distribution with low dispersity ($Đ$ = 1.08) (**Fig. 2a**). The block length ratio between PEG, PGC(EPC) and PGC(EC) of the block terpolymer **3** was determined by ^{1}H NMR spectroscopy to be 45:37:56 by comparing the integration of the methylene protons resonating at 3.63 ppm from the macroinitiator PEG with the integrations of the proton resonances at 3.40 ppm from methoxy groups and at 2.58 ppm from the terminal alkynes in the PGC segments (**Fig. 2b**).

The alkyne-containing polymer **1** was further reacted with MPA in the presence of photoinitiator 2,2-dimethoxy-2-phenylacetophenone (DMPA) under UV irradiation for 2 h to afford the carboxylic acid-functionalized block terpolymer **2** (**Scheme S2**). The reaction mixture was transferred to dialysis tubing and dialyzed against nanopure water at room temperature for 3 d to remove excess thiol and solvent residues, followed by lyophilization. The polymer was re-dissolved in THF and precipitated into diethyl ether to remove DMPA residues, then dried under vacuum to yield block terpolymer **2** as a white powder. The disappearance of the proton resonance at 2.58 ppm in the ^{1}H NMR spectrum, as shown in **Fig. S2b**, demonstrated the successful consumption of the terminal alkynyl groups during the post-polymerization modification *via* thiol-yne click chemistry. Fourier transform infrared (FT-IR) spectroscopy further supported that this reaction had occurred together with the introduction of carboxylic acid groups by the appearance of a broad O-H stretching band from 3700 to 3000 cm^{-1} coincident with the disappearance of a sharper alkynyl C-H stretch at 3300 cm^{-1} (**Fig. S2a**).

The DOPA-functionalized block terpolymer **3** was obtained by amidation of the carboxylic acids on **2** with dopamine, as shown in **Scheme 1 and Scheme S3**.[65] Polymer **2** and dopamine hydrochloride were allowed to undergo reaction at 0 °C in the presence of 1-ethyl-3-(3-dimethylaminopropyl)-1-ethyl-carbodiimide hydrochloride (EDC hydrochloride) and triethyl amine in anhydrous DMF. The reaction vessel was under continuous nitrogen flow and wrapped with aluminium foil to avoid potential side reactions, *e.g.* polymerization of dopamine. FT-IR spectroscopy showed a shift of a portion of the C=O stretch intensity from 1750 cm^{-1} to 1660 cm^{-1} upon amidation, corresponding to transformation of the carboxylic acids to amides with retention of the carbonate carbonyl groups (**Fig. S3a**). The appearance of resonances from the dopamine aromatic protons between 6.25 – 6.75 ppm in the ^{1}H NMR spectrum (**Fig. S3b**), indicated *ca.* 50% functionalization of the carboxylic acids of the polymer backbone by dopamine moieties.

Taken together, these results demonstrated the successful synthesis of the sugar-based amphiphilic triblock terpolymer **3**, having the complex compositional profile illustrated in **Scheme 1**.

Co-assembly of MIONs and sugar-based polymeric scaffolds

The co-assembly of MIONs and **3** was performed through a solvent exchange process, modified from previous reports (**Fig. 3a**).[34, 66] The block lengths of the PEG and PGC-based blocks were tuned to balance the dispersion in water and interactions of dopamine with MIONs. MIONs and **3** were first dispersed in THF and DMF, respectively, to form homogeneously-distributed solutions. The two solutions were thoroughly mixed at a volume ratio of 1:1 by vortex and sonication to afford a clear brown mixture. Afterwards, nanopure water (2× relative to organic solution volume) was added dropwise *via* a syringe pump, followed by a rapid addition of another 2× nanopure water, where the water served as a selective poor solvent for both the hydrophobic PGC(EC) block and the MIONs, inducing the formation of micelles with capture of the nanoparticles. This technique was hypothesized to first allow quasi-equilibrium assembly through slow addition, and then kinetically trap the morphology *via* rapid addition.[67, 68] Excess organic solvent was then removed by dialysis against nanopure water for 24 h. Finally, the magnetic nanocomposite solution was lyophilized to yield a brown powder. TEM analysis showed that each globular polymeric micelle had encapsulated multiple MIONs with a D_{av} of 160 ± 40 nm, after measuring > 50 nanoparticles (**Fig. 3b**). Dark-field scanning transmission electron microscopy (STEM) and elemental mapping measurements were performed on the MION-loaded nanocomposites using an energy-dispersive X-ray spectroscopy (EDS) detector showing the co-localization of iron oxide and nanocomposites, according to the iron (Fe) intensity profile and dark field STEM images, respectively, which further demonstrated that MIONs were loaded into the polymeric matrix (**Fig. S5a-d**). In addition, thermogravimetric analysis (TGA) of MIONs and **3** under nitrogen atmosphere showed less than 30% and more than 90% mass loss for MIONs and polymeric scaffold upon heating to 500 °C, respectively, whereas the nanocomposites were found to retain 20% of mass, suggesting *ca.* 20% thermally stable inorganic components were contained inside the nanocomposites (**Fig. S5e**). Narrowly dispersed nanocomposites with a number-average hydrodynamic diameter (D_h(number)) of 140 ± 50 nm were also observed by dynamic light scattering (DLS). The slightly larger dry-state diameter measured by TEM is expected to be caused by some degree of deformation upon deposition and drying on the carbon-coated copper grid for TEM imaging (**Fig. 3c**). Further support for reorganization and flattening of the globular nanostructures on substrates was found by measurement of an average height of *ca.* 17.6 ± 1.7 nm by atomic force microscopy (AFM) (**Fig. S4**).

Quantitative evaluation of crude oil loading capacity and recyclability of the sugar-based magnetic nanocomposites.

Following the full characterization of the sugar-based magnetic nanocomposites, their ability to sequester complex oil pollutants was assessed qualitatively and quantitatively. Crude oil (density = *ca.* 0.76 mg/mL) was obtained from the Texas-Oklahoma Enbridge pipeline and then weathered according to a previously established procedure.[69] As shown in **Fig. 4a**, firstly, several drops of crude oil were added to water in order to mimic the oil sheen on the water surface. Secondly, lyophilized samples of sugar-based magnetic nanocomposites were applied, which floated on the surface. Within several seconds, the nanocomposites had uptaken sufficient crude oil to breakup the oil sheen, as shown in the video of **Fig. S7** included in the Supporting Information. Results from experiments that are shown by the panels of images captured within **Fig. 4b** and **4c** indicated that the crude oil-loaded nanocomposites were capable of following the motion of the external magnet remotely (see also the video of **Fig. S8**), eventually being separated from the water together with the oil pollutants. Quantitative oil sequestration experiments were also pursued by deploying the lyophilized nanocomposite powder to crude oil-contaminated water samples at nanocomposite/crude oil (mg/μL) ratios of 1:5, 1:10, 1:15, 1:20, 1:25, and 1:30 (**Fig. 5a**, **Table S1**). The nanocomposite-oil-water mixtures were allowed to stand for *ca.* 10 h, a time period far in excess of that needed to reach a visually-apparent steady state of crude oil capture. As the crude oil was taken up by the magnetic nanocomposites, the oil layer on the surface of the water diminished while the originally light brown nanocomposite powder darkened in colour (**Fig. 4a-c** and **Fig. S7**). Quantitative assessments were performed after an external magnet (neodymium magnet, 90 lb pull) was used to attract the loaded nanocomposites. A rapid magnetic response was observed – just several seconds were required to collect the

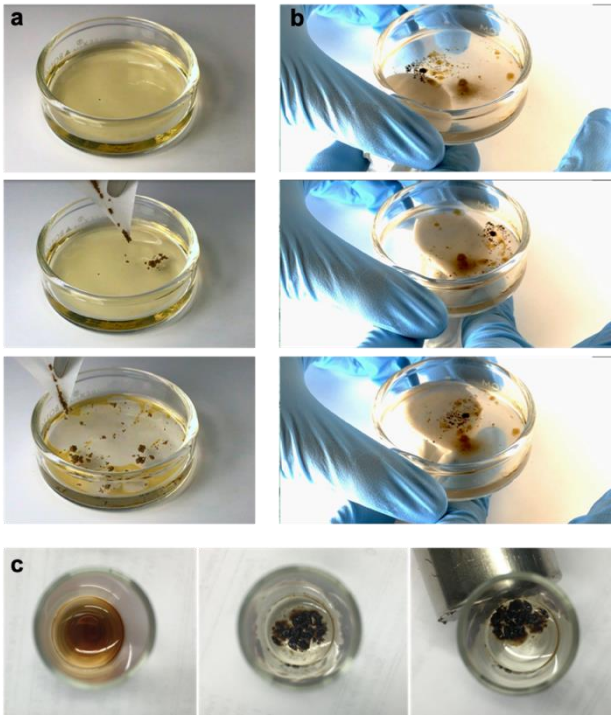

Fig. 4 Representative photographs of (a) crude oil sheen before and during addition of nanocomposites **4**, (b) the crude oil-loaded nanocomposites **4** attracted by a moving magnet at the bottom of the container, and (c) quantitative oil sequestration experiments showing that the vial containing crude-oil contaminated water before and after oil sorption by **4**. (Videos illustrating (a) and (b) are available in the Supporting Information.)

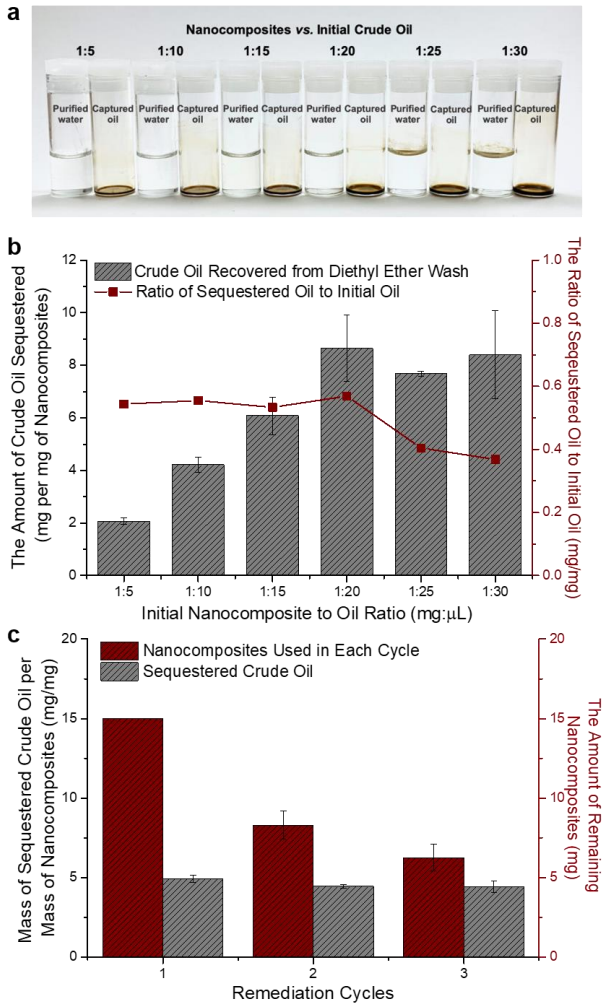

Fig. 5 Quantitative evaluation of crude oil loading capacity and recyclability: (a) Photograph of recovered crude oil (left) and purified water (right) with different nanocomposites-to-crude oil ratios; (b) the amount of crude oil sequestered by nanocomposites **4** with different initial nanocomposites-to-crude oil ratios; (c) recycling performance of nanocomposites **4** evaluated by comparing the total amount of crude oil sequestered, nanocomposites used in each cycle, and crude oil sequestered per unit mass of nanocomposites **4**.

nanocomposites and decant the purified water into a new vial. The loaded nanocomposites were then washed twice with diethyl ether to extract the crude oil and the magnet was used to collect the recovered nanocomposites. The resulting crude oil and diethyl ether mixture was transferred to another pre-weighed clean vial and concentrated. The amounts of crude oil pollutants captured by nanocomposites were thereby quantified. **Fig. 5b** shows that the crude oil uptake ability of the nanocomposites increased significantly from 1:5, 1:10, 1:15, to 1:20 of initial nanocomposite-to-oil ratio, then increased slowly when higher excesses of crude oil were deployed. Based on the results from sequestration experiments using 1:20, 1:25 and 1:30 initial nanocomposite-to-oil ratios, the sugar-based nanocomposites were able to recover 8× to 9× their initial dry weight of crude oil pollutants.

Recyclability of the nanocomposites was assessed by repeating the oil sequestration experiments for three cycles. The amount of crude oil used for each cycle was set as 150 μL and the initial nanocomposite was 15 mg. It was noted that 60 – 80 wt% of the nanocomposites were able to be retrieved each cycle, the loss of which was due to the sacrifice during deployment and organic solvent washing (**Fig. 5c**, **Table S2**). It was observed that the loading capacity of the reused nanocomposites maintained at *ca.* 5 mg/mg, suggesting the potential of sugar-based magnetic nanocomposites as recyclable agents for crude oil sequestration.

Degradation study in organic media, aqueous media, and an environmental chamber

Due to the fact that some of the nanocomposites may not be retrieved, it was pivotal to further study their degradation profile under different environmental conditions. A series of studies was performed over months in organic solvent, water, and an environmental chamber to simulate the degradation process of the nanocomposites in crude oil, aqueous media, and climatic conditions (**Fig. 6** and **S6**).

The degradation of **3** was investigated using ^{1}H NMR spectroscopy following incubation at 37 °C under basic conditions in D_2O and DMSO-d_6. A pristine polymer sample was dissolved into D_2O and DMSO-d_6 (5 mg/mL) containing NaOD and triethylamine, respectively. In both conditions, sharp peaks appeared and accumulated over time, as shown in **Fig. S6**, suggesting the generation of oligomers and small molecules from the original polymer backbone. The degradation products were analysed by electrospray ionisation mass spectrometry (ESI-MS), as shown in **Fig. 6a**-**b**. Additionally, environmental chamber testing was conducted to expose nanocomposites **4** to the climatic conditions that simulate the temperature and humidity of the Texas Gulf Coast, with an average annual temperature of 22 °C and an average annual relative humidity (RH) of 70%.[70] After retrieval of the loaded nanocomposites, the mixture of unrecovered crude oil and remaining nanocomposites in water was analysed by ESI-MS (**Fig. 6c**). The ESI-MS analysis shown in **Fig. 6a-c** suggested that the sugar-based polymer degraded into moieties with smaller molar masses, and the possible degradation products were presumed based on cleavage of labile carbonate backbone and carbonate, ester and amide side chain linkages in the presence of aqueous NaOH, as well as oxidation of thioethers into sulfoxides and sulfones during this long period of degradation.[71, 72] The final degradation products and corresponding mechanism are under further investigation.

Conclusions

With an urgent need to develop sustainable and environmentally-friendly materials to tackle the threat of crude oil pollution, magnetically-responsive nanocomposites derived from sugar were designed and studied. By merging polymer materials and nanotechnology, this composite material served as nano-sized carriers for pollutant absorption. It was observed that these sugar-based magnetic nanocomposites act as a dispersible agent to effectively absorb crude oil nearly ten-fold their initial dry weight. Besides, the nanocomposites are able

to carry versatile functionalities by virtue of the scalable and translatable chemical synthetic approach, enabling their utilization in the clean-up of other polluted resources. For example, fracking produced water has long been facing a major disposal challenge, given their large volumes as well as high levels of salinity, toxic metals, and radioactivity.[73] Upon modification with chelating agents, such as ethylenediaminetetraacetic acid, the nanocomposites hold promise for this problem. Furthermore, the pollutant-loaded composite materials can be remotely controlled and reused for multiple cycles, thereby, increasing their resource efficiency and lowering their energy and economic costs. Moreover, their degradability allows these nanocomposites to eventually break down into their natural building blocks and derivative small molecules, alleviating the production and persistence of microplastics. Therefore, the design of this material makes a significant contribution not only in pollution control and resource recovery, but also in developing a roadmap from our existing linear economy, towards a more sustainable and resource-efficient circular plastics economy.

Conflicts of interest

There are no conflicts to declare.

Author information

Corresponding Author
*E-mail: wooley@chem.tamu.edu.

ORCID:
Mei Dong: 0000-0002-9862-0296
Yue Song: 000-0002-7800-5528
Hai Wang: 0000-0002-1215-2613
Lu Su: 0000-0001-8207-756X
Yen-Nan Lin: 0000-0001-71118-7771
Rachel A. Letteri: 0000-0002-2919-203X
Jialuo Li: 0000-0001-9760-4983
Karen L. Wooley: 0000-0003-4086-384X

Acknowledgements

We gratefully acknowledge financial support from the National Science Foundation under grant numbers CHE-1610311, DMREF-1629094 and DMR-1905818, and the Welch Foundation through the W. T. Doherty- Welch Chair in Chemistry under grant number A-0001. Enbridge Energy Partners, L.P. is acknowledged for their generous donation of the West Texas crude oil, *via* Mr. Jonathan Sanders. Besides, we thank Mr. Haomiao Xie (Department of Chemistry, Texas A&M University) for his assistance with SQUID and Dr. Hong-Cai Zhou (Department of Chemistry, Texas A&M University) for his support with the STEM-EDS mapping studies. STEM-EDS analyses were supported by the National Science Foundation Small Business Innovation Research (NSF-SBIR) program under grant number 1632486 and the Robert A. Welch Foundation through a Welch Endowed Chair to H.C.Z. (A-0030).

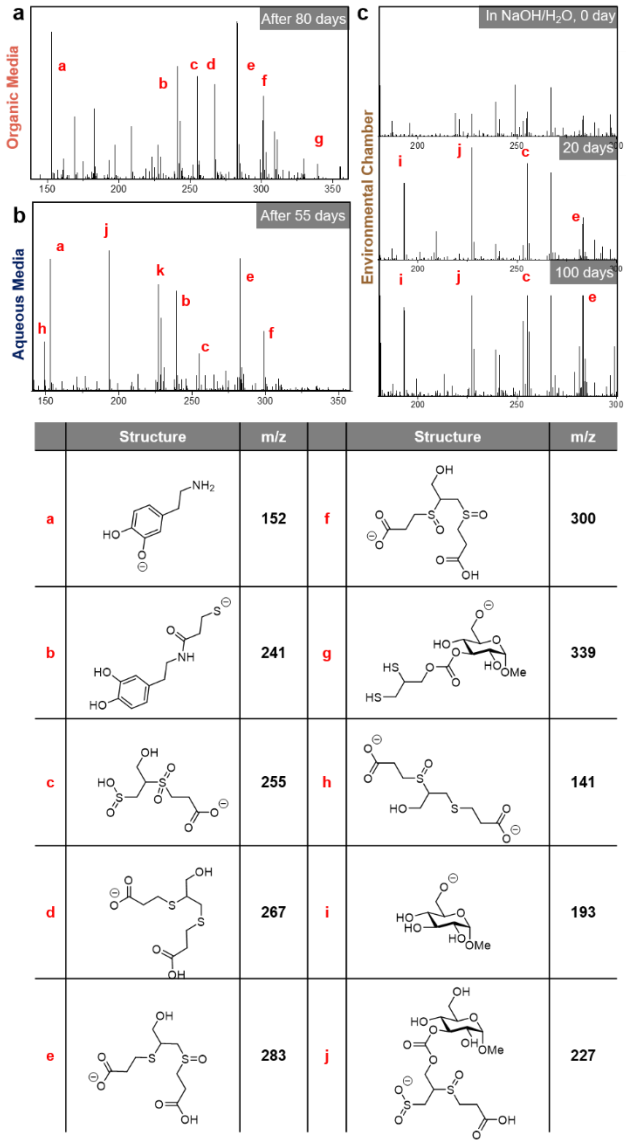

Fig. 6 ESI-MS analysis of the degradation products of (a) triblock terpolymer **3** in DMSO-d_6 (5 mg/mL) with addition of D_2O (20% vol/vol) and triethylamine (6 mg/mL) during incubation with shaking at 37 °C over a period of 80 days; (b) triblock terpolymer **3** in D_2O (5 mg/mL) with addition of NaOD adjusted to pH 10 during incubation with shaking at 37 °C over a period of 55 days; (c) nanocomposites **4** in H_2O (5 mg/mL) with addition of NaOH adjusted to pH 8 in an environmental chamber (T = 22 °C, RH = 70%) over 100 days. Mass spectra are in negative-ion mode.

Notes and references

1. P. F. Kingston, *Spill Sci. Technol. Bull.*, 2002, **7**, 53-61.
2. S. A. Patin, *Environmental Impact of the Offshore Oil and Gas Industry*, JSTOR, 1999.
3. G. Gordon, I. Stavi, U. Shavit and R. Rosenzweig, *Geoderma*, 2018, **312**, 114-120.
4. M. Fingas, *The Basics of Oil Spill Cleanup*, CRC press, 2012.
5. R. Z. Hoff, *Mar. Pollut. Bull.*, 1993, **26**, 476-481.
6. U. S. E. P. A. O. o. E. a. R. Response., *Understanding Oil Spills And Oil Spill Response*, 1999.

7. R. R. Lessard and G. DeMarco, *Spill Sci. Technol. Bull.*, 2000, **6**, 59-68.
8. A. Bayat, S. F. Aghamiri, A. Moheb and G. R. Vakili-Nezhaad, *Chem. Eng. Technol.*, 2005, **28**, 1525-1528.
9. G. Canevari, *United States Patent* 1974, No. 3,793,218.
10. L. S. Fendall and M. A. Sewell, *Mar. Pollut. Bull.*, 2009, **58**, 1225-1228.
11. M. Eriksen, L. C. Lebreton, H. S. Carson, M. Thiel, C. J. Moore, J. C. Borerro, F. Galgani, P. G. Ryan and J. Reisser, *PloS one*, 2014, **9**, e111913.
12. F. M. Windsor, I. Durance, A. A. Horton, R. C. Thompson, C. R. Tyler and S. J. Ormerod, *Global Change Biol.*, 2019, **25**, 1207-1221.
13. L. Van Cauwenberghe, A. Vanreusel, J. Mees and C. R. Janssen, *Environ. Pollut.*, 2013, **182**, 495-499.
14. A. L. Andrady, *Mar. Pollut. Bull.*, 2011, **62**, 1596-1605.
15. K. Ng and J. Obbard, *Mar. Pollut. Bull.*, 2006, **52**, 761-767.
16. R. d. C. F. Silva, D. G. Almeida, R. D. Rufino, J. M. Luna, V. A. Santos and L. A. Sarubbo, *Int. J. Mol. Sci.*, 2014, **15**, 12523-12542.
17. M. Cole, P. Lindeque, E. Fileman, C. Halsband, R. Goodhead, J. Moger and T. S. Galloway, *Environ. Sci. Technol.*, 2013, **47**, 6646-6655.
18. H. Nguyen, M. Stuchtey and M. Zils, *McKinsey Quarterly*, 2014, **1**, 46-63.
19. S. Huysman, J. De Schaepmeester, K. Ragaert, J. Dewulf and S. De Meester, *Resour., Conserv. Recycl.*, 2017, **120**, 46-54.
20. E. Van Eygen, D. Laner and J. Fellner, *Waste Manage. (Oxford)*, 2018, **72**, 55-64.
21. W. R. Stahel, *Nature News*, 2016, **531**, 435.
22. H. M. Choi and R. M. Cloud, *Environ. Sci. Technol.*, 1992, **26**, 772-776.
23. H. Zhu, S. Qiu, W. Jiang, D. Wu and C. Zhang, *Environ. Sci. Technol.*, 2011, **45**, 4527-4531.
24. J. Ge, H. Y. Zhao, H. W. Zhu, J. Huang, L. A. Shi and S. H. Yu, *Adv. Mater.*, 2016, **28**, 10459-10490.
25. L. Xiao, Y. Ling, A. Alsbaiee, C. Li, D. E. Helbling and W. R. Dichtel, *J. Am. Chem. Soc.*, 2017, **139**, 7689-7692.
26. P. Calcagnile, D. Fragouli, I. S. Bayer, G. C. Anyfantis, L. Martiradonna, P. D. Cozzoli, R. Cingolani and A. Athanassiou, *ACS Nano*, 2012, **6**, 5413-5419.
27. J. Pyun, *Polym. Rev.*, 2007, **47**, 231-263.
28. X. Gui, Z. Zeng, Z. Lin, Q. Gan, R. Xiang, Y. Zhu, A. Cao and Z. Tang, *ACS Appl. Mater. Interfaces*, 2013, **5**, 5845-5850.
29. B. Ge, X. Zhu, Y. Li, X. Men, P. Li and Z. Zhang, *Colloids Surf., A*, 2015, **482**, 687-692.
30. K. Y. Yoon, Z. Li, B. M. Neilson, W. Lee, C. Huh, S. L. Bryant, C. W. Bielawski and K. P. Johnston, *Macromolecules*, 2012, **45**, 5157-5166.
31. N. Chen and Q. Pan, *ACS nano*, 2013, **7**, 6875-6883.
32. W. Lehr, H. Cekirge, R. Fraga and M. Belen, *Oil Petrochem. Pollut.*, 1984, **2**, 7-11.
33. J. A. Fay, in *Oil on the Sea*, Springer, 1969, pp. 53-63.
34. A. Pavía-Sanders, S. Zhang, J. A. Flores, J. E. Sanders, J. E. Raymond and K. L. Wooley, *ACS Nano*, 2013, **7**, 7552-7561.
35. J. A. Flores, A. Pavía-Sanders, Y. Chen, D. J. Pochan and K. L. Wooley, *Chem. Mater.*, 2015, **27**, 3775-3782.
36. M. Fingas and C. Brown, *Mar. Pollut. Bull.*, 2014, **83**, 9-23.
37. K. A. Kvenvolden and C. K. Cooper, *Geo-Mar. Lett.*, 2003, **23**, 140-146.
38. M. Blumer, *Science*, 1972, **176**, 1257-1258.
39. E. B. Kujawinski, M. C. Kido Soule, D. L. Valentine, A. K. Boysen, K. Longnecker and M. C. Redmond, *Environ. Sci. Technol.*, 2011, **45**, 1298-1306.
40. M. L. Pedrotti, S. Petit, A. Elineau, S. Bruzaud, J.-C. Crebassa, B. Dumontet, E. Martí, G. Gorsky and A. Cózar, *PloS one*, 2016, **11**, e0161581.
41. L. Su, R. Li, S. Khan, R. Clanton, F. Zhang, Y.-N. Lin, Y. Song, H. Wang, J. Fan and S. Hernandez, *J. Am. Chem. Soc.*, 2018, **140**, 1438-1446.
42. Y. Song, X. Ji, M. Dong, R. Li, Y.-N. Lin, H. Wang and K. L. Wooley, *J. Am. Chem. Soc.*, 2018, **140**, 16053-16057.
43. Y.-N. Lin, L. Su, J. Smolen, R. Li, Y. Song, H. Wang, M. Dong and K. L. Wooley, *Mater. Chem. Front.*, 2018, **2**, 2230-2238.
44. B. G. G. Lohmeijer, R. C. Pratt, F. Leibfarth, J. W. Logan, D. A. Long, A. P. Dove, F. Nederberg, J. Choi, C. Wade, R. M. Waymouth and J. L. Hedrick, *Macromolecules*, 2006, **39**, 8574-8583.
45. R. C. Pratt, B. G. G. Lohmeijer, D. A. Long, R. M. Waymouth and J. L. Hedrick, *J. Am. Chem. Soc.*, 2006, **128**, 4556-4557.
46. C. L. Maikawa, A. Sevit, B. Lin, R. J. Wallstrom, J. L. Mann, A. C. Yu, R. M. Waymouth and E. A. Appel, *J. Polym. Sci., Part A: Polym. Chem.*, 2019, **57**, 1322-1332.
47. K. Mikami, A. T. Lonnecker, T. P. Gustafson, N. F. Zinnel, P.-J. Pai, D. H. Russell and K. L. Wooley, *J. Am. Chem. Soc.*, 2013, **135**, 6826-6829.
48. S. E. Felder, M. J. Redding, A. Noel, S. M. Grayson and K. L. Wooley, *Macromolecules*, 2018, **51**, 1787-1797.
49. L. Su, S. Khan, J. Fan, Y.-N. Lin, H. Wang, T. P. Gustafson, F. Zhang and K. L. Wooley, *Polym. Chem.*, 2017, **8**, 1699-1707.
50. G. L. Gregory, E. M. López-Vidal and A. Buchard, *Chem. Commun.*, 2017, **53**, 2198-2217.
51. T. M. McGuire, E. M. López-Vidal, G. L. Gregory and A. Buchard, *J. CO_2 Util.*, 2018, **27**, 283-288.
52. G. L. Gregory, G. Kociok-Köhn and A. Buchard, *Polym. Chem.*, 2017, **8**, 2093-2104.
53. Y. Shen, X. Chen and R. A. Gross, *Macromolecules*, 1999, **32**, 2799-2802.
54. D. Pati, X. Feng, N. Hadjichristidis and Y. Gnanou, *Macromolecules*, 2017, **50**, 1362-1370.
55. A. Beharaj, E. Z. McCaslin, W. A. Blessing and M. W. Grinstaff, *Nat. Commun.*, 2019, **10**, 5478.
56. N. Fanjul-Mosteirín, C. Jehanno, F. Ruipérez, H. Sardon and A. P. Dove, *ACS Sustainable Chem. Eng.*, 2019, **7**, 10633-10640.
57. L. X. Chen, T. Liu, M. C. Thurnauer, R. Csencsits and T. Rajh, *J. Phys. Chem. B*, 2002, **106**, 8539-8546.
58. C. Xu, K. Xu, H. Gu, R. Zheng, H. Liu, X. Zhang, Z. Guo and B. Xu, *J. Am. Chem. Soc.*, 2004, **126**, 9938-9939.
59. G. Schmidt, B. R. Hamaker and J. J. Wilker, *Adv. Sustainable Syst.*, 2018, **2**, 1700159.
60. H. C. Kolb, M. G. Finn and K. B. Sharpless, *Angew. Chem. Int. Ed.*, 2001, **40**, 2004-2021.
61. C. E. Hoyle, T. Y. Lee and T. Roper, *J. Polym. Sci., Part A: Polym. Chem.*, 2004, **42**, 5301-5338.
62. K. L. Killops, L. M. Campos and C. J. Hawker, *J. Am. Chem. Soc.*, 2008, **130**, 5062-5064.
63. S. Sun, H. Zeng, D. B. Robinson, S. Raoux, P. M. Rice, S. X. Wang and G. Li, *J. Am. Chem. Soc.*, 2004, **126**, 273-279.
64. N. Bao, L. Shen, Y. Wang, P. Padhan and A. Gupta, *J. Am. Chem. Soc.*, 2007, **129**, 12374-12375.

65. Z. Li, G. Davidson-Rozenfeld, M. Vázquez-González, M. Fadeev, J. Zhang, H. Tian and I. Willner, *J. Am. Chem. Soc.*, 2018, **140**, 17691-17701.
66. B.-S. Kim, J.-M. Qiu, J.-P. Wang and T. A. Taton, *Nano Lett.*, 2005, **5**, 1987-1991.
67. D. J. Beltran-Villegas and A. Jayaraman, *J. Chem. Eng. Data*, 2018, **63**, 2351-2367.
68. L.-T. Yan and X.-M. Xie, *Prog. Polym. Sci.*, 2013, **38**, 369-405.
69. B. Lehr, S. Bristol and A. Possolo, Oil Budget Calculator: Deepwater Horizon, https://www.restorethegulf.gov/sites/default/files/documents/pdf/OilBudgetCalc_Full_HQ-Print_111110.pdf, (accessed 2/10/2020).
70. National Oceanic and Atmospheric Administration (NOAA), Climate Data Online Search, https://www.climate.gov/maps-data/dataset/past-weather-zip-code-data-table, (accessed 2/10/2020).
71. I. Barnes, V. Bastian, K. H. Becker, E. H. Fink and W. Nelsen, *J. Atmos. Chem.*, 1986, **4**, 445-466.
72. C. Schoeneich, A. Aced and K. D. Asmus, *J. Am. Chem. Soc.*, 1993, **115**, 11376-11383.
73. N. R. Warner, C. A. Christie, R. B. Jackson and A. Vengosh, *Environ. Sci. Technol.*, 2013, **47**, 11849-11857.

TOC: